JOURNAL OF MATERIALS SCIENCE **38** (2003) 4193–4201

Spatially resolved thermal diffusivity measurements on functionally graded materials

A. NEUBRAND*
Fraunhofer Institut für Werkstoffmechanik, Wöhlerstr. 11, D-79108 Freiburg, Germany
E-mail: neu@iwm.fhg.de

H. BECKER
Schott Lithotec AG, Jerusalemer Str. 13, D-98617 Meiningen, Germany

T. TSCHUDI
Darmstadt University of Technology, Institute of Applied Physics, Hochschulstr. 6, D-64289 Darmstadt, Germany

Photothermal generation of thermal waves was used in combination with the probe beam deflection technique to study the thermal diffusivity of functionally graded materials (FGMs) quantitatively. An amplitude modulated Ar ion laser was used as a heat source and the HeNe probe laser was reflected from the specimen surface at almost normal incidence. It is demonstrated that this measuring technique can be used for a precise determination of the thermal diffusivity for a wide variety of materials if appropriate measuring conditions are chosen. The precision of the thermal diffusivity measurement was better than 5% for all materials studied. The achieved spatial resolution of the thermal diffusivity measurement was about 100 μm, but higher spatial resolutions can be achieved if necessary. In a graded Al_2O_3/Al composite local fluctuations of the thermal diffusivity were observed due to the coarseness of the microstructure, but the overall behaviour of the thermal conductivity could be described well by the Maxwell-Eucken relationship. In a functionally graded AlCu alloy, a smooth thermal diffusivity profile was observed in the region where the alloy consisted of a solid solution of Cu in Al.

1. Introduction

In a functionally graded material (FGM) spatially inhomogeneous properties are introduced intentionally, usually by composition gradients. These gradients can reduce thermomechanical stresses and avoid stress singularities at materials interfaces [1, 2]. Analytical [3] or numerical [4] calculations of the stresses in the FGM serve to optimize the composition gradient thus minimizing the thermal stresses and maximizing lifetime. In many of their potential applications such as thermal barrier coatings, reentry materials, fuel cells, thermoelectric converters or evaporator tubes functionally graded components are subjected to heat fluxes [5, 6], and thermophysical property data as a function of position are required as input parameters for the aforementioned calculations. For the description of nonstationary heat flow in a material both the thermal diffusivity a and the thermal conductivity λ are necessary. These two quantities are linked by

$$\lambda = c_p \rho a \tag{1}$$

where c_p is the specific heat capacity (in J/kg) and ρ is the density of the material. Standard measurement techniques for thermal conductivity include the guarded hot plate [7], the calorimeter [8] and the hot wire method [9]. Thermal diffusivities are usually measured with the radial heat flow [10] or the laser flash [11] method. These methods require large homogeneous specimens and thermal diffusivity or conductivity data for a graded material can only be obtained if homogeneous reference specimens with the compositions found in the FGM are used such as in [12]. As the thermal diffusivity depends strongly on pores, microcracks and microstructure, which may be altered during production or service of the graded component, the validity of the data obtained from homogeneous reference specimens has to be carefully verified. Such limitations call for methods which are capable of a spatially resolved measurement of thermal properties which can be performed directly on the graded material. One method which provides spatial resolution is infrared thermography, which has been used to measure the thermal conductivity profile in various metal/ceramic FGMs [13]. In this particular experiment, a cylindrical specimen with the gradient along the cylinder axis was used. The specimen was heated from the top face, and the steady-state temperature profile along the central axis of the specimen was

*Author to whom all correspondence should be addressed.

measured by an infrared camera and converted to a thermal conductivity profile. The thermography method has the drawback of requiring a large specimen of a suitable geometry. Therefore the laser flash method was modified in such a way that the temperature rise is not recorded for the whole back of the specimen, but for a small region [14]. This method will only yield meaningful results if the specimen thickness is much less than the extension of the graded region. According to ASTM E1461-92 [15] the thickness of a specimen for the laser flash method should not be less than 1.5 mm, and therefore the spatial resolution of this method is insufficient for many FGMs.

Photodeflectance [16] and photoreflectance [17] microscopy offer a high spatial resolution which makes thermal measurements on single grains possible [18]. These techniques use one laser beam (pump laser) which is periodically modulated with angular frequency ω to heat the speciman and one weaker laser beam (probe laser) to detect the produced thermal gradients through the optical beam deflection effect. In the most common of these techniques, the mirage technique in the skimming regime [19], the second laser beam travels parallel to the heated surface at a height z_0 and the deflection is caused by the temperature gradient in the air above the heated spot. The major drawback of the mirage technique is the necessity that the height z_0 be smaller than the thermal diffusion length

$$l = \sqrt{\frac{2a}{\omega}} \tag{2}$$

For specimens with a low thermal diffusivity this requirement is difficult to fulfill, and the deflection is completely controlled by heat diffusion in air. It has therefore been proposed to use the so-called bouncing method [20] for thermal diffusivity measurements. The probe beam is reflected from the surface close to the heating zone at a small angle and small thermal diffusivities can be measured with this method [21]. However, the conversion of the measured beam deflection to a thermal diffusivity requires comprehensive calculations as the beam deflection in the air is superimposed to that caused by the surface deformation due to the thermal expansion of the specimen. In this work, a complementary method is presented where the probe laser beam is reflected from the specimen surface at almost normal incidence. It will be shown that this method allows a precise determination of the thermal diffusivity in various materials without extensive numeric evaluation of the data if certain conditions are met. The method is used to determine the thermal diffusivity of various graded materials as a function of position.

2. Measurement of thermal diffusivity by probe deflection

The principle of the employed photothermal setup is shown in Fig. 1. The light intensity of a pump laser is periodically modulated with angular frequency ω and heats the specimen. Thermal expansion of the heated region causes deformation of the specimen surface from which a second weak laser beam is reflected. The

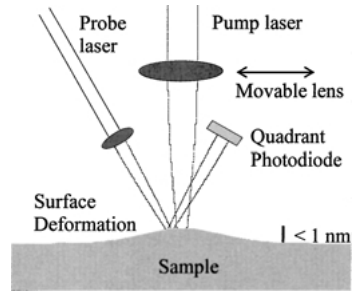

Figure 1 Principle of photothermal beam deflection experiment: A pump laser heats the specimen surface periodically. The surface deforms thermoelastically, and the non-stationary part of the deformation is probed by the deflection of a probe laser beam.

non-stationary component of the surface deformation causes a deflection of the probe laser beam which oscillates with the modulation frequency ω. The amplitude and phase of the deflection signal is recorded as a function of distance from the heating spot and used to extract information on the thermal diffusivity of the specimen. For this purpose the heat conduction equation for the given problem must be solved and the resulting surface deformation must be calculated.

2.1. Solution of the heat conduction equation

A cartesian coordinate system with the sample surface at $z = 0$ is chosen (Fig. 2). For our purpose, the differential equations for heat conduction and the elastic deformation can be decoupled and the Fourier heat transfer equation

$$\Delta T - \frac{1}{a}\dot{T} = -\frac{Q}{\lambda} \tag{3}$$

can be solved independently. T denotes temperature and Q is the source term of the heat conduction equation. If the heat source is a pump laser beam impinging perpendicularly on the specimen surface at $x, y = 0$ with a Gaussian intensity distribution of width a_1 modulated with angular frequency ω

$$Q(x, y, z, t) = \frac{2 \cdot \alpha_1 \cdot P_0}{\pi a_1^2} \exp\left(-2\frac{x^2 + y^2}{a_1^2}\right) \times \exp(\alpha_1 z) \exp(i\omega t) \tag{4}$$

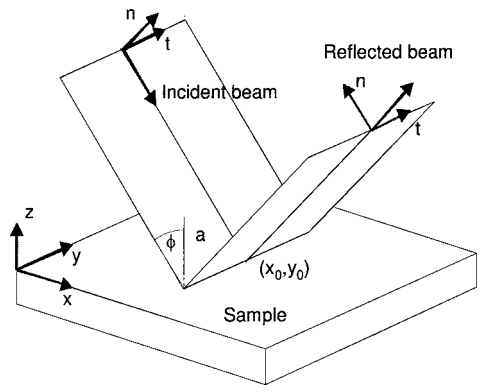

Figure 2 Parameters describing the incident and reflected probe laser beam and employed coordinate system.

P_0 is the absorbed laser power and α_1 is the absorption coefficient of the laser radiation in the specimen material. Substituting (2) into (1) the heat conduction equation for the specimen becomes:

$$\Delta T_s(x, y, z) - \frac{i\omega}{a_s} T_s(x, y, z) = -\frac{\frac{2\cdot\alpha_1\cdot P_0}{\pi a_1^2} \exp\left(-2\frac{x^2+y^2}{a_1^2}\right) \exp(\alpha_1 z)}{\lambda_s} \exp(i\omega t) \quad (5)$$

where a_s and λ_s denote the thermal diffusivity and conductivity of the specimen, respectively. The temperature distribution $T_g(x, y, z)$ in the air above the specimen needs to satisfy the following differential equation:

$$\Delta T_g - \frac{i\omega}{a_g} T_g(x, y, z) = 0 \quad (6)$$

where a_g is the thermal diffusivity of air. The boundary conditions of this differential equation are identical temperature of specimen and air at $z = 0$

$$T_s(x, y, z = 0) = T_g(x, y, z = 0) \quad (7)$$

and identical heat flux perpendicular to the surface

$$\lambda_s \frac{\partial T_s}{\partial z}\bigg|_{z=0} = \lambda_g \frac{\partial T_g}{\partial z}\bigg|_{z=0} \quad (8)$$

λ_g denotes the thermal conductivity of air. For a semi-infinite specimen in a semi-infinite medium

$$\lim_{z\to-\infty} T_s = \lim_{z\to\infty} T_g = 0 \quad (9)$$

For these boundary conditions the non-stationary part of the temperature distribution in the specimen $T_s(x, y, z, t)$ becomes:

$$T_s(x, y, z, t) = \frac{\alpha_1 P_0}{4\pi^2} \exp(i\omega t) \int_{-\infty}^{\infty}\int_{-\infty}^{\infty} \frac{\exp[i(\delta_x x + \delta_y y)]}{\lambda_s\left(\beta_s^2 - \alpha_1^2\right)} \times \exp\left(-a_1^2 \frac{\delta_x^2 + \delta_y^2}{8}\right) x \times \left[\exp(\alpha_1 z) - \frac{(\lambda_g\beta_g + \lambda_s\alpha_1)}{(\lambda_g\beta_g + \lambda_s\beta_s)} \exp(\beta_s z)\right] d\delta_x\, d\delta_y \quad (10)$$

TABLE I Parameters used for the calculation of temperature profiles and the probe beam deflection

	Copper	Fused silica	Air
Radius of heating laser beam $a_1(\mu m)$	30	30	30
Absorbed laser power (W)	1	1	
Angle of incidence of probe laser φ	20	20	20
Thermal diffusivity (cm^2/s)	0.939	0.0085	0.215
Thermal conductivity (W/m*K)	395	1.36	
Thermal expansion coefficient (10^{-6}/K)	16.8	0.45	
Poisson ratio	0.35	0.17	

The non-stationary part of the temperature distribution in the air becomes:

$$T_g(x, y, z, t) = \frac{\alpha_1 P_1}{4\pi^2} \exp(i\omega t) \times \int_{-\infty}^{\infty}\int_{-\infty}^{\infty} \left[\frac{\exp(-\beta_g z) \exp[i(\delta_x x + \delta_y y)]}{(\lambda_g\beta_g + \lambda_s\beta_s)(\beta_s + \alpha_1)} \times \exp\left(-a_1^2 \frac{\delta_x^2 + \delta_y^2}{8}\right)\right] d\delta_x\, d\delta_y \quad (11)$$

with

$$\beta_{s,g} = \sqrt{\delta_x^2 + \delta_y^2 + \frac{i\omega}{a_{s,g}}} \quad (12)$$

Examples of temperature distributions were calculated for copper and fused silica employing the parameters shown in Table I. It was assumed that the fused silica surface was coated with an opaque thin film. The oscillatory part of the temperature distribution in the sample and in the air is plotted in Fig. 3 for copper and silica glass as examples of high and low thermal diffusivity materials. It is obvious that the isophase lines in the solid material are concentric circles whereas the

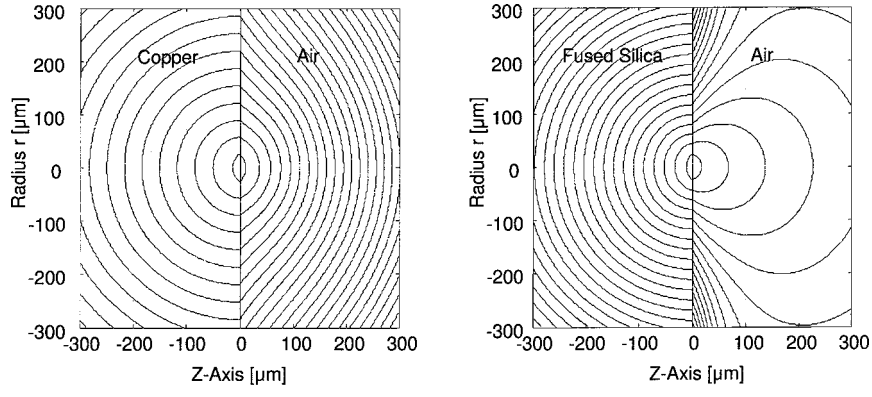

(a) (b)

Figure 3 Calculated isophase lines of the oscillating part of the temperature for 31 Hz modulation frequency. (a) Copper in air (phase shift between isolines is 0.03 rad). (b) Fused silica in air (phase shift between isolines is 0.2 rad).

isophase lines in air deviate from semicircles in the vicinity of the specimen. This shape of the isophase lines is typical for a strongly absorbing material which has a much higher heat capacity per volume than air. In this case the temperature distribution in the specimen is almost unaffected by the air surrounding it.

2.2. Probe beam deflection at the specimen surface

The heating beam causes an axisymmetric surface deformation. The probe beam is reflected from the surface at a position x_0, y_0 with an angle φ to the surface normal (Fig. 2). It is assumed that the probe ray travels parallel to the x axis. The normal component of the deflection Φ_n caused by the inclination of the specimen surface is then given by

$$\Phi_n = -2x_0 \frac{du_z}{dr}\bigg|_{z=0} = -\frac{2mx_0}{r} \tag{13}$$

where $r = \sqrt{(x_0^2 + y_0^2)}$ is the distance from the centre of the heated spot, U_z is the normal displacement of the specimen surface, and the inclination m is the derivate of the surface displacement in r as illustrated in Fig. 4. Introducing the temperature distribution inside the specimen T_s into the Navier-Stokes equation the following result for the inclination of the surface m is obtained [21]

$$m(r) = \frac{-(1+\nu)\alpha_{th}\alpha_l P_0}{\pi\lambda_s} \exp(i\omega t) \times \int_0^\infty \frac{\delta^2 J_1(\delta r)\exp\left(-\frac{\delta a_1)^2}{8}\right)[\lambda_s(\alpha_l+\delta+\beta_s)+\lambda_g\beta_g]}{(\lambda_s\beta_s+\lambda_g\beta_g)(\beta_s+\delta)(\alpha_l+\delta)(\beta_s+\alpha_l)}\, d\delta \tag{14}$$

where α_{th} and ν are the thermal expansion coefficient and Poisson ratio of the specimen, respectively and J_1 denotes the first order Bessel function. Note that m is a complex quantity describing both the amplitude and the phase of the deflection signal. If the experimental arrangement is such that $y_0 = 0$ then $x_0 = r$ and the signal from the differential amplifier S is proportional to the displacement

$$S(r) \propto \Phi_n(r) = 2m(r) \tag{15}$$

The amplitude of the signal is proportional to the thermal expansion coefficient and the absorbed laser power. The integral in (14) introduces a phase shift between the pump laser and the deflection signal which depends on the distance r between the heating and the probe beam and the material properties α_l, β_s, β_g, λ_s and λ_g.

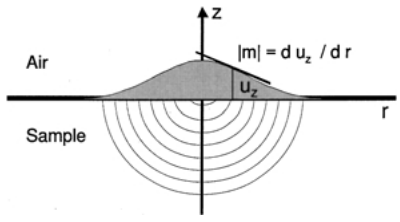

Figure 4 Sketch of the thermoelastic surface deformation and the inclination of the surface m.

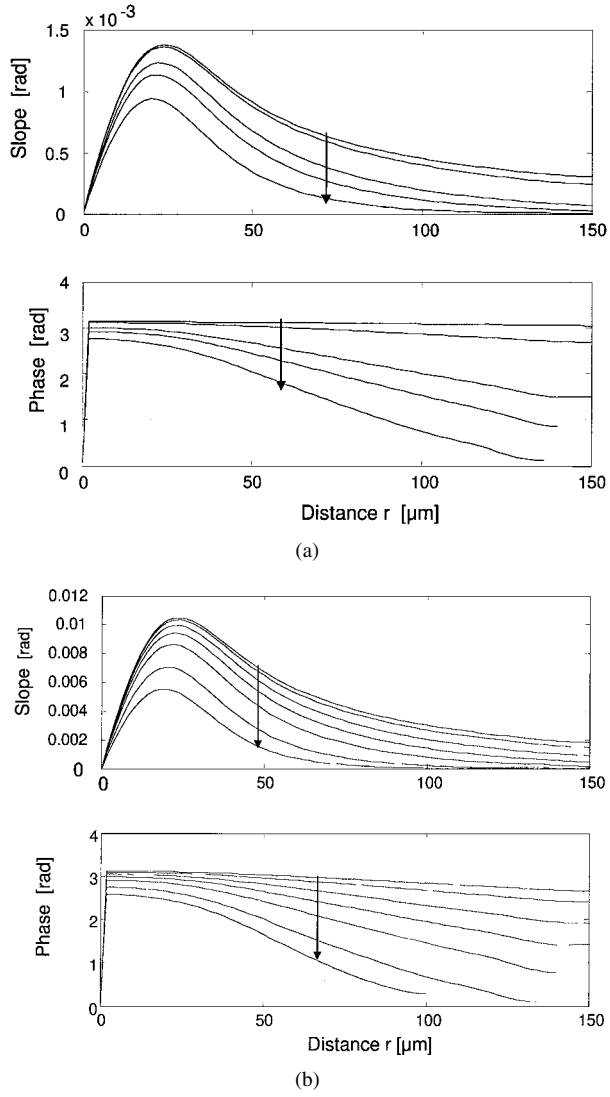

Figure 5 Calculated amplitude and phase of the beam deflection signal for different modulation frequencies. The parameters reproduced in Table I were used for the calculation. (a) Copper (modulation frequencies 100, 1000, 10000, 20000 and 50000 Hz in the order indicated by the arrow) and (b) Fused silica (modulation frequencies 10, 20, 50, 100, 200, 500 and 1000 Hz in the order indicated by the arrow).

Fig. 5 shows the calcuated amplitude and phase of the beam deflection for a copper and a fused silica specimen. The amplitude reaches a maximum at $r \approx 30\ \mu$m corresponding to the waist of the laser beam. The deflection decays with increasing r, the decay for large frequencies being faster. The maximum amplitude is only reached for frequencies where the thermal diffusion length is much larger than the radius of the heating laser spot. For copper this frequency corresponds to 1000 Hz, for fused silica it is 20 Hz. The phase of the deflection shows an approximately linear decrease for intermediate distances which are larger than the radius of the heating laser beam. For the copper specimen deviations from linearity are only visible at the highest frequency (50 kHz) and distances above 100 μm corresponding to four thermal wavelengths. For the fused silica specimen deviations from linearity are also predicted for distances which exceed 4 times the thermal diffusion length. They are clearly visible

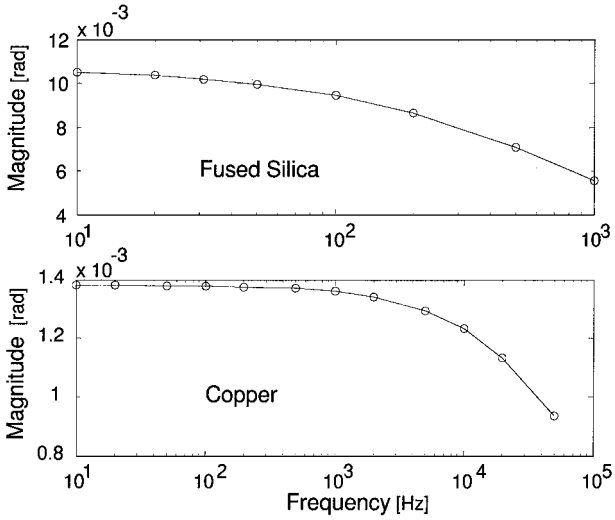

Figure 6 Maximum periodic beam deflection due to surface deformation for fused silica and copper. The parameters reproduced in Table I were used for the calculation.

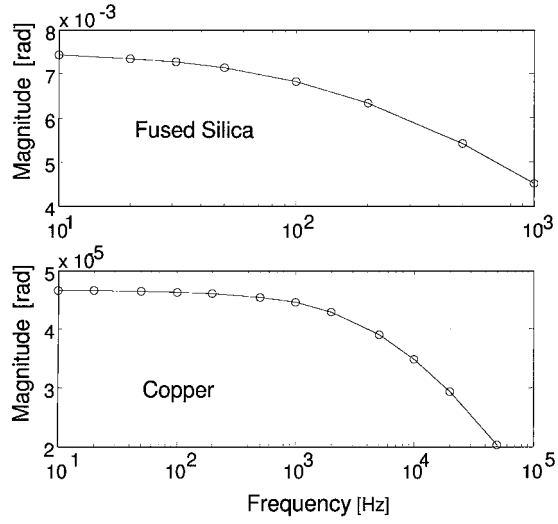

Figure 7 Maximum periodic beam deflection due to the refractive index gradient in air above a fused silica and above a copper sample. The parameters reproduced in Table I were used for the calculation.

for 1000 Hz modulation frequency where the thermal diffusion length is only 16 μm.

The maximum deflection amplitude for different frequencies is plotted in Fig. 6 for copper and fused silica. In fused silica, the maximum signal amplitude at low frequences is about 8 times higher than in copper despite of the 40 times lower thermal expansion coefficient of fused silica compared to copper. The effects of the thermal expansion coefficient are overcompensated by the extremely low thermal conductivity of silica which is only 1/300 of copper. As a result the heated region reaches a much higher temperature in silica leading to a larger surface deformation.

2.3. Probe beam deflection by the temperature gradient in the air

As the experiment is carried out in air, the probe beam is not only deflected by the surface, but also by the refractive index gradient caused by the temperature distribution in the air above the sample. The normal component of this deflection is given by[22]

$$\Phi_{\mathrm{n}} = -\frac{1}{n_{\mathrm{g}}}\left(\frac{\mathrm{d}n_{\mathrm{g}}}{\mathrm{d}T}\right)\frac{\alpha_1 P_0 \tan^2\varphi}{2\pi^2}\exp(i\omega t) \times \int_{-\infty}^{\infty}\int_{-\infty}^{\infty}\exp\left(-a_1^2\frac{\delta_x^2\delta_y^2}{8}\right)\exp[i(\delta_{\mathrm{x}}x_0+\delta_{\mathrm{y}}y_0)] \; x\,\frac{i\delta_{\mathrm{x}}\beta_{\mathrm{g}}}{\left(\beta_{\mathrm{g}}^2+\delta_{\mathrm{x}}^2\tan^2\varphi\right)(\lambda_{\mathrm{g}}\beta_{\mathrm{g}}+\lambda_{\mathrm{s}}\beta_{\mathrm{s}})(\beta_{\mathrm{s}}+\alpha_1)}\,\mathrm{d}\delta_{\mathrm{x}}\,\mathrm{d}\delta_{\mathrm{y}} \tag{16}$$

The amplitude of the signal is proportional to the derivative of the refractive index with temperature and the absorbed laser power. It is important to note that there is a dependence of deflection on the angle of incidence—the beam deflection becomes small for a small angle φ.

Fig. 7 shows the calculated maximum deflection amplitude caused by the temperature gradient in air for a copper and a fused silica specimen for identical conditions as in Fig. 6. For fused silica the maximum deflection of the probe beam in the air above the specimen is 7.5 mrad and comparable to the deflection caused by the surface deformation. For copper the maximum deflection in the air is about 0.047 mrad and thus hardly 4% of that caused by the surface deformation. For experimental arrangement with almost normal incidence of the probe beam (small angle φ) the beam deflection in air can thus be neglected if the specimen has a moderate or large thermal expansion coefficient.

2.4. Determination of thermal diffusivity

In cases where the beam deflection is almost exclusively caused by the surface deformation, it is possible to extract β_{s} and the thermal diffusivity of the specimen from a measurement of the amplitude or phase of m as a function of distance according to (14) (the parameters α_1, β_{g}, λ_{s} and λ_{g} must be known). The evaluation of the thermal conductivity can be simplified if the assumption is made that the thermal conductivity of the sample is much larger than that of air, and that the absorption coefficient is much larger than the reciprocal of the thermal diffusion length. In this case $\lambda_{\mathrm{g}}\beta_{\mathrm{g}} \ll \lambda_{\mathrm{s}}\beta_{\mathrm{s}}$ and $\beta_{\mathrm{s}} \ll \alpha_1$, and for all values of δ where the integrand is not close to zero (14) can then simplified to

$$m(r) = \frac{-(1+\nu)\alpha_{\mathrm{th}}\alpha_1 P_0}{\pi\lambda_{\mathrm{s}}}\exp(i\omega t) \times \int_0^{\infty}\frac{\delta^2 J_1(\delta r)\exp\left(-\frac{(\delta a_1)^2}{8}\right)}{\beta_{\mathrm{s}}(\beta_{\mathrm{s}}+\delta)}\mathrm{d}\delta \tag{17}$$

The phase of the signal depends only on the value of the integral in (17), and therefore it is possible to extract the parameter β_{s} and thus the thermal conductivity from the phase of the signal as a function of position without knowledge of the absorption coefficients and heat capacities of the materials involved.

2.5. Experimental procedure

The experimental setup for the probe beam deflection measurement is shown in Fig. 8. An Ar-ion laser was

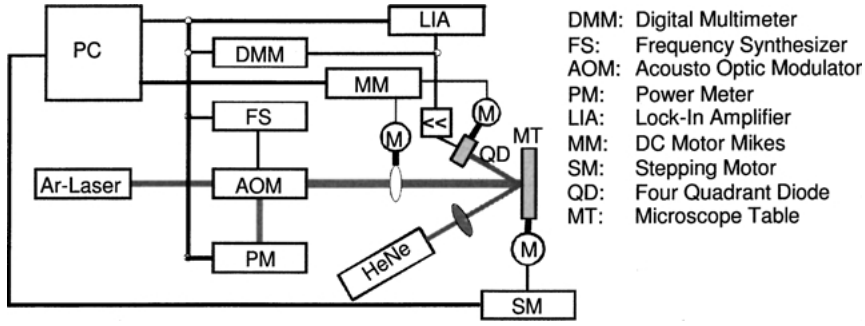

Figure 8 Block diagram of the main components of the experimental setup.

amplitude modulated by an acousto-optic modulator and focused onto the sample surface. The thermoelastic surface deformation was probed by a focused HeNe laser beam reflected from the surface. The deflection of the probe laser was measured using a four quadrant photodiode connected to a differential preamplifier and lock-in amplifier combination. A personal computer equipped with an IEEE488 interface recorded the laser power and the phase and amplitude of the lock-in signal. It also controlled the settings of the lock-in amplifier, frequency synthesizer and stepping motors positioning the four quadrant photodiode, the specimen, and the lens focussing the pump laser. The movement of the latter in small steps allowed movement of the pump laser beam relative to the probe laser. In this way the phase shift of the surface deformation relative to the pump laser beam could be measured as a function of distance. Further details of the experimental setup can be found in an earlier work [22].

The graded AlCu alloy was produced by directed solidification of AlCu4 in a vertical Bridgman furnace. Natural thermosolutal convection was used to homogenize the melt. Details of the process are described in [23]. The copper concentration gradient in the graded alloy was determined in a scanning electron microscope equipped with EDX. The Al_2O_3/Al-FGM was prepared using a foam replication method described in Reference [24]. All samples were ground and polished prior to the measurement. The graded composite was additionally coated with a thin film (<1 μm) of aluminium to improve its reflectivity. For reference measurements of the thermal diffusivity, the specimens were coated with a thin carbon coating and measured in a laser flash apparatus (Hoffmann GmbH, Leimersheim, Germany).

3. Results and discussion

For the determination of the thermal diffusivity of the specimens only the phase shift of the oscillatory part of the beam deflection was measured as a function of distance r from the heated spot. The experimentally measured phase as a function of distance showed a slope which could be fitted very well with a straight line for r above 50 μm and below four thermal wavelenths as illustrated in Fig. 9 for a copper specimen. The standard deviation of the plot of phase versus distance r from a straight line was 0.53°. The experimental observation is thus in good agreement with the theoretical

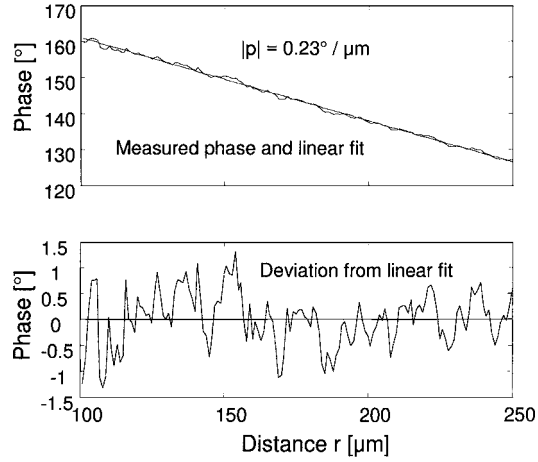

Figure 9 Illustration of a phase measurement on electrolytic Cu at 1.2 kHz modulation frequency. Above: Measured phase and fitted linear fit with slope $|p| = 0.23°/\mu$m are almost indistinguishable. Below: Deviation of the measured phase from the linear fit (enlarged).

predictions of the previous section. The relative uncertainty of the slope of the fitted straight line $\Delta p/p$ is only 1.5% indicating a similar precision of the thermal diffusivity values derived from this slope. Fig. 10 shows the slope of the phase $p = -\Delta\phi/\Delta r$ for the same electrolytic copper sample and different modulation frequencies. The complex integral in (14) was evaluated numerically, and the phase of the signal was fitted for different frequencies using different values

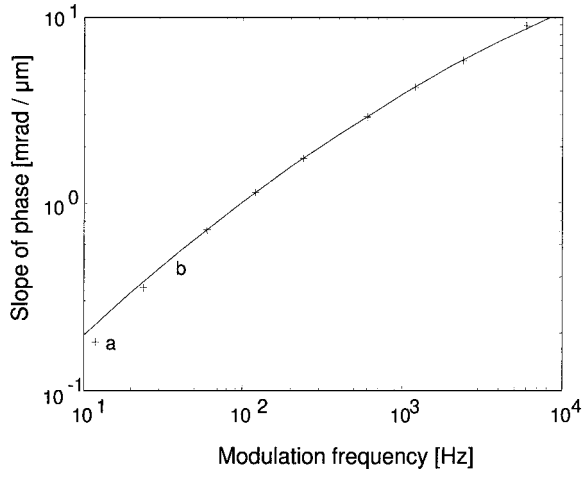

Figure 10 Slope of the phase p for electrolytic Cu. Data points (a): Measured slope of the phase for different frequencies. Line (b): Predicted slope of the phase using (14) and a thermal diffusivity $a = 1.08$ cm^2/s.

of the thermal diffusivity. Using a single thermal diffusivity value of 1.08 cm^2/s the measured slope of the phase p could be predicted very well for all modulation frequencies. This indicates that the employed method yields meaningful thermal diffusivity values for a wide range of modulation frequencies.

The goal of the present work was to evaluate the thermal diffusivity as a function of position in a graded material. The application of the previously described method for the data evaluation would mean a large computational effort for the determination of the thermal diffusivity profile of one graded specimen. It was thus tried to use the so called phase method to simplify the evaluation of the phase plot (Fig. 9). This method employs the slope p in the linear region of the diagram phase ϕ versus offset r to calculate a characteristic length $l_c = -\Delta r/\Delta\phi = 1/p$. Numerical analysis of (14) shows that this characteristic length is not equal to the thermal diffusion length l for the surface deflection problem even if the effect of the air on the thermal wave in the specimen is negligible. The characteristic length differs from the thermal wavelength by a factor γ that depends on the optical absorption coefficient α_l. γ approaches 1.45 if the absorption coefficient α_l is large compared to the reciprocal thermal wavelength [21]. If the factor γ is known, the thermal diffusivity of the specimen can be calculated from the characteristic length l_c determined from the linear region of the phase plot according to:

$$a = \frac{\omega}{2} \cdot \left(\frac{l_c}{\gamma}\right)^2 \tag{18}$$

In our experiments, the correct value for the thermal diffusivity 1.08 cm^2/s could be retained from the slope $p = 1/l_c$ of the linear region of the phase plot using (18) for modulation frequencies between 250 Hz and 4 kHz, if γ was set to 1.41. This is in good agreement with the numerically calculated value of 1.45 for the linear region of the phase plot and large absorption coefficients α_l. The small deviation from $\gamma = 1.45$ is probably due to a small offset of the scan line relative to the x-axis. This causes an apparent decrease in l_c which must be compensated by a slightly lower value of γ. As the geometrical arrangement of the laser beams was the same in all experiments a value of $\gamma = 1.41$ was used for thermal diffusivity determinations employing (18). It should be mentioned that the diffusivity retained using (18) would be higher than the actual one for modulation frequencies where the thermal diffusion length is very different from the scan distance r. Qualitatively this can be understood looking at Fig. 5 which shows that the slope of the phase is lower for small or large ratios of thermal wavelength to distance. Obviously only the intermediate region where the slope of the phase is almost exactly linear should be evaluated.

In order to check the precision of the thermal diffusivity values received with the probe beam deflection technique using (18) and $\gamma = 1.41$, a set of commercially available Cu, Al and Fe alloys with a wide range of thermal diffusivities between 0.01 cm^2/s and 1 cm^2/s was investigated (Table II). The obtained results are compared with the laser flash method according to ASTM E 1461-92 [15]. The statistical error calculated from the standard deviation of the laser flash measurement is 2% for the lower thermal diffusivity samples rising to 5% for the copper alloy. The values determined using the probe beam deflection technique are in excellent agreement with the laser flash results if the uncertainty of the laser flash measurements is taken into account. It is concluded that thermal diffusivity values calculated with (18) are precise if the laser radiation of the pump laser is absorbed at the specimen surface and a measurement frequency is used such that the distance of the probe beam corresponds to approximately one thermal wavelength.

TABLE II Comparison of thermal diffusivity values determined with the laser-flash method [15] and the probe beam deflection method (this work). All values in cm^2/s. Reproduced laser-flash values are the mean of 20 measurements

	Laser-flash method	Probe beam deflection
Copper	0.939 ± 0.047	0.935 ± 0.021
Aluminium	0.567 ± 0.017	0.570 ± 0.012
Brass	0.342 ± 0.008	0.330 ± 0.006
Iron	0.174 ± 0.004	0.164 ± 0.004
Steel	0.039 ± 0.001	0.040 ± 0.001

The thermal diffusivity of a Al_2O_3/Al FGM with a linear aluminium concentration profile from 31.1% to 3.9% was measured as a function of position using the probe beam deflection technique (Fig. 11). The FGM specimen was coated with a thin film of 0.5 μm Al in order to improve its reflectivity and faciliate the measurement. Reference measurements with metals which could be measured with and without Al film proved that such a thin coating did not affect the thermal wave propagation for the thermal wavelengths investigated. The thermal diffusivity values of the Al_2O_3/Al FGM show the same trend as the composition profile (Fig. 11). It is interesting to note that the thermal diffusivity shows fluctuations even in the region of the composite with a constant composition. These fluctuations are much larger than the standard deviation of the measured diffusivity in a homogeneous material. They are thus a real property of the investigated composite which consists of metal channels of about 40 μm diameter and a ceramic phase of similar size. At metal volume fractions below 30% it is likely that only few metal channels are found in the volume investigated in a single measurement, and statistical fluctuations of the number, size and

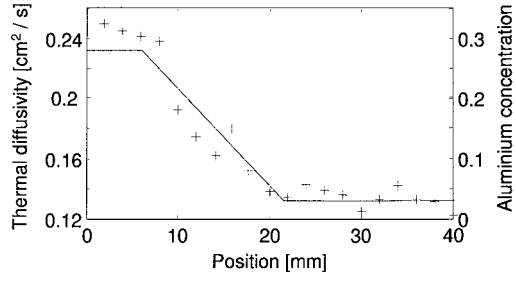

Figure 11 Spatially resolved thermal diffusivity measurement of a functionally graded Al_2O_3/Al composite. + Measured thermal diffusivity values; — Aluminium concentration profile.

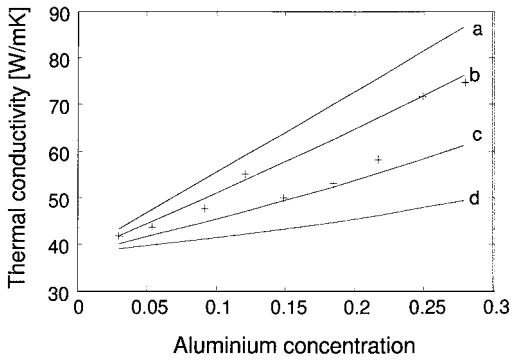

Figure 12 Thermal conductivity of Al_2O_3/Al as a function of composition. + Measured thermal conductivity value. The lines are predictions of different rules of mixture: (a) Voigt, (b) Maxwell-Eucken (upper bound), (c) Maxwell-Eucken (lower bound), and (d) Reuss.

orientation of the aluminium ligaments lead to fluctuations in thermal diffusivity.

The measured thermal diffusivity was converted to thermal conductivity using (1) and a linear rule of mixture for the heat capacity and density of the composite (if interface energies and residual porosity in the composite are neglected the linear rule of mixture follows directly from the conservation of mass and energy). The plot of thermal conductivity against the volume fraction of Al is shown in Fig. 12. Although there is some scatter in the experimental conductivity data due to the aforementioned reasons, all values fall between the upper and lower Maxwell-Eucken bounds for the thermal conductivity. This agreement indicates that the graded composite prepared by the GMFC method does not contain microcracks or porosity. Measured values of the Young's modulus in these Al_2O_3/Al FGMs match a rule-of-mixtures for interpenetrating network microstructures which also confirms the absence of porosity [24].

As a second example the thermal diffusivity of a graded Al-Cu alloy prepared by directional solidification was determined. The copper concentration gradient in the alloy is displayed in Fig. 13. The composition on the left corresponds to the original unmolten AlCu4 alloy. In the molten zone, which was solidified from the left to the right, the copper content slowly increases from 0.7% to about 6%. The measured thermal

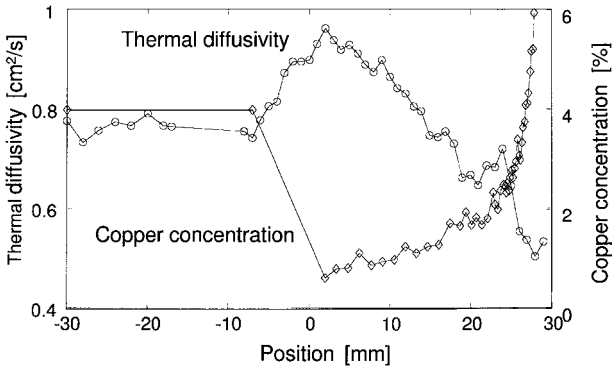

Figure 13 Spatially resolved thermal diffusivity measurement of a functionally graded AlCu alloy. ○, Measured thermal diffusivity values; ◇, copper concentration profile as measured by EDX. Lines are guides for the eye only.

diffusivity reflects these changes in Cu concentration: The thermal diffusivity in the unmolten AlCu4 region was determined as 0.75 cm^2/s with very little change. As the Cu content decreases the measured diffusivity increases. This is due to the fact that the AlCu alloy forms a solid solution in this concentration range and the Cu atoms on Al sites effectively reduce the electric and thermal conductivity of the alloy. The maximum value of thermal diffusivity of 0.88 cm^2/s is thus observed at the lowest Cu concentration of 0.7%. This thermal diffusivity value is very close to the literature value for pure Al of 0.89 cm^2/s. During the directed solidification process the Cu concentration increases again and, as a consequence the thermal conductivity decreases to a value of 0.5 cm^2/s. The irregularity in the thermal diffusivity of the sample near $x = 24$ mm is caused by the fact that the forced convection inside the Bridgman furnace became unstable as the thickness of the molten zone decreases. The unstable convection causes local fluctuations in Cu concentration and thermal conductivity.

4. Conclusions

A non-contact thermal wave setup for the quantitative and spatially resolved determination of the thermal diffusivity was developed. An amplitude modulated heating laser was used for the generation of thermal waves. The thermal waves caused a thermoelastic surface deformation which was probed by deflection of a weak probe laser beam. It was demonstrated that the thermal diffusivity of a specimen can be determined precisely by numerical evaluation of the phase of the deflection signal as a function of position. For optically dense specimens, the analytic expression (18) also yielded thermal diffusivity data with an accuracy of better than 5% if the thermal diffusivity was higher than 0.04 cm^2/s and the modulation frequency was chosen such that the thermal wavelength was in the range of several diameters of the diameter of the heating laser beam. The spatial resolution of the measurements was about 100 μm. Although possible, a higher resolution was not intended for the present experiments, because the resolution would have become comparable to the characteristic length scale of the microstructure of the investigated composites. Measurements on Al_2O_3/Al FGMs which have a coarse microstructure nevertheless showed considerable local fluctuations of the thermal diffusivity. The thermal conductivity of the graded Al_2O_3/Al composites obeyed the Maxwell-Eucken relationship indicating negligible porosity and micro-cracking. The thermal diffusivity profile of a graded AlCu alloy corresponded well with the Cu concentration profile measured by EDX. It is concluded that photothermal beam deflection is a powerful tool for quantitative and spatially resolved thermal diffusivity measurements.

Acknowledgements

We are indebted to Dr. B. Siber and PD Dr. M. Rettenmayr for supplying the graded AlCu alloy and to T.J. Chung for preparation of the graded Al_2O_3/Al specimen.

References

1. Chapter, "Functionally Graded Materials," in "Encyclopedia of Materials: Science and Technology" (Elsevier Science, Oxford, 2001).
2. N. CHERRADI, A. KAWASKI and M. GASIK, *Comp. Eng.* **4** (1994) 883.
3. K. S. RAVICHANDRAN, *Mater. Sci. Eng.* **A201** (1994) 269.
4. J. R. CHO and D. Y. HA, *ibid*. **A302** (2001) 187.
5. M. TAKAHASHI, Y. ITOH and M. MIYAZAKI, in Proceedings of Thermal Spraying ITSC'95 (High Temperature Society of Japan, 1995) p. 83.
6. Y. MIYAMOTO, in Functionally Graded Materials: Proceedings of the International Symposium on Manufacture, Properties, and Applications of Functionally Graded Materials, 1996 (American Ceramic Society, Westerville, Ohio, 1997) p. 171.
7. Standard Test Method for Steady State Heat Flux Measurements and Thermal Transmission Properties by Means of the Guarded Hot Plate Apparatus, ASTM C177-85, "Annual Book of Standards" (American Society for Testing and Materials, Philadelphia, PA, 1990) Vol. 14.01.
8. Standard Test Method for Thermal Conductivity of Refractories, ASTM C201-86, "Annual Book of Standards" (American Society for Testing and Materials, Philadelphia, PA, 1990) Vol. 15.01.
9. W. E. HAUPIN, *Amer. Ceram. Soc. Bull.* **39** (1960) 139.
10. J. A. CAPE, G. W. LEHMAN and M. M. NAKATA, *J. Appl. Phys*. **34** (1963) 3550.
11. R. E. TAYLOR, *High Temperatures-High Pressures* **11** (1979) 43.
12. R. WATANABE, A. KAWASAKI, M. TANAKA and J.-F. LI, *Int. J. Refr. Hard Mater.* **12** (1994) 187.
13. T. ISHIZUKA, S. OKADA and K. WAKASHIMA, in Proc. of the FGM Symposium 1994, edited by B. Ilschner and N. Cherradi (Presses Polytechniques et Universitaires Romandes, Switzerland, 1995) p. 453.
14. T. BABA, T. MATSUMOTO, A. ONO and T. SANO, in FGM'90, Proc. of the 1st International Symposium on Functionally Gradient Materials 1990, edited by M. Yamanouchi, M. Koizumi, T. Hirai, and I. Shiota (FGM Forum, Tokyo, 1990) p. 285.
15. Standard Test Method for Thermal Diffusivity of Solids by the Flash Method, ASTM E 1461-92.
16. K. PLAMANN and D. FOURNIER, *Phys. Stat. Sol.*(a) **154** (1996) 351.
17. L. FABBRI, D. FOURNIER, L. POTTIER and L. ESPOSITO, *J. Mater. Sci.* **31** (1996) 5429.
18. B. LI, L. POTTIER, J. P. ROGER, D. FOURNIER, K. WATARI and K. HIRATO, *J. Eur. Ceram. Soc.* **19** (1999) 1631.
19. A. SALAZAR, A. SANCHEZ-LAVEGA, A. OCARIZ, J. GUITONNY, G. C. PANDEY, D. FOURNIER and A. C. BOCCARA, *J. Appl. Phys.* **79** (1996) 3984.
20. M. BERTOLOTTI, G. LIAKHOU, R. LI VOTI, F. MICHELOTTI and C. SIBILIA, *ibid.* **74** (1993) 7078.
21. M. BERTOLOTTI, O. LIAKHOU and R. LI VOTI, *ibid.* **83** (1998) 966.
22. H. W. BECKER, in Einsatz Photothermischer Strahlablenkung zur Charakterisierung dünner optischer Schichten und Bestimmung des Temperaturleitwerts von Gradien- tenwerkstoffen, Ph.D. Thesis, University of Technology Darmstadt 2000, http://elib.tudarmstadt.de/diss/000068/
23. B. SIBER, M. RETTENMAYR and C. MÜLLER, in "Functionally Graded Materials 1998, Materials Science Forum 308-311," edited by W.A. Kaysser (TransTech, Switzerland, 1999) p. 211.
24. A. NEUBRAND, T.-J. CHUNG, E. D. STEFFLER, T. FETT and J. RÖDEL, *J. Mater. Res.* **17** (2002) 2912.

Received 28 January
and accepted 23 July 2003